

THE 1-JETTINESS EVENT-SHAPE FOR DIS WITH NNLL RESUMMATION

ZHONG-BO KANG

Los Alamos National Laboratory, Theoretical Division, Los Alamos, NM 87545, USA

XIAOHUI LIU

*High Energy Division, Argonne National Laboratory, Argonne, IL 60439, USA
 Department of Physics and Astronomy, Northwestern University, Evanston, IL 60208, USA*

SONNY MANTRY*

*High Energy Division, Argonne National Laboratory, Argonne, IL 60439, USA
 Department of Physics and Astronomy, Northwestern University, Evanston, IL 60208, USA*

JIANWEI QIU

*Physics Department, Brookhaven National Laboratory, Upton, NY 11973
 C.N. Yang Institute for Theoretical Physics, Stony Brook University, Stony Brook, NY 11794*

We propose the use of 1-jettiness, a global event shape, for exclusive single jet production in lepton-nucleus deep inelastic scattering (DIS). We derive a factorization formula, using the Soft-Collinear Effective Theory, differential in the transverse momentum and rapidity of the jet and the 1-jettiness event shape. It provides a quantitative measure of the shape of the final-state QCD radiation in the presence of the hard jet, providing a useful powerful probe of QCD and nuclear physics. For example, one expects differences in the observed pattern of QCD radiation between large and small nuclei and these can be quantified by the 1-jettiness event shape. Numerical results are given for this new DIS event shape at leading twist with resummation at the next-to-next-to-leading logarithmic (NNLL) level of accuracy, for a variety of nuclear targets. Such studies would be ideal at a future EIC or LHeC electron-ion collider, where a range of nuclear targets are planned.

Keywords: DIS; 1-jettiness; Event Shapes.

PACS numbers: 11.25.Hf, 123.1K

1. Introduction

It is well-known that global event shapes, such as thrust distributions at e^+e^- colliders, have played a vital role in furthering our understanding of QCD. The concept of event shapes for DIS was first introduced and developed^{1,2,3,4} more than a decade ago. Thrust¹ and Broadening³ distributions were studied at the next-to-leading-log (NLL) level of accuracy and matched at $\mathcal{O}(\alpha_s)$ to fixed order results. A

*Talk presented at the QCD Evolution Workshop, JLab, May 6th-10th, 2013.

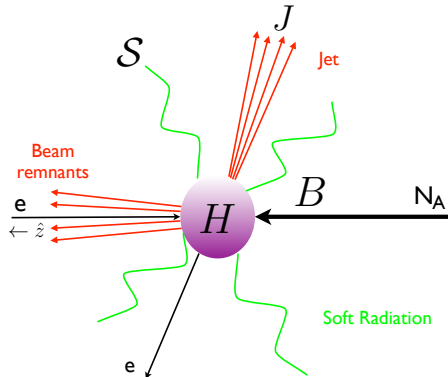


Fig. 1. Schematic figure of the process $e^- + N_A \rightarrow J + X$ in the limit $\tau_1 \ll P_{J_T}$. The restriction $\tau_1 \ll P_{J_T}$ allows only soft radiation of energy $E \sim \tau_1$ between the beam and jet directions. The factorization framework for this process is schematically shown in Eqs. (9) and (10).

numerical comparison was also done against $\mathcal{O}(\alpha_s^2)$ results^{5,6}. Thrust distributions have also been measured at HERA by the H1^{7,8,9} and ZEUS^{10,11,12} collaborations.

In this work we use N-Jettiness¹³, a global event shape for exclusive N-jet production, to study single jet production in electron-nucleus collisions

$$e^- + N_A \rightarrow J + X, \quad (1)$$

where N_A denotes a nucleus of atomic weight A and J denotes the leading final-state jet. The additional hadronic radiation, contained in X , will be highly restricted (see Fig.1) for small values of the 1-jettiness (τ_1) event shape. τ_1 distributions provide theoretical control over the amount of radiation between the beam and jet directions, which can be used as a probe of QCD and nuclear medium effects. N-Jettiness¹³ was first introduced in the context of implementing jet vetoes at hadron colliders and has now been applied to several processes^{14,15,16,17}. We adapt this technology to exclusive jet production in deep-inelastic scattering (DIS).

The use of 1-jettiness as a DIS event shape to probe of QCD and nuclear dynamics was first proposed in Ref. 18. In particular, the 1-jettiness event shape observable, for the process in Eq.(1), was defined as

$$d\sigma_A \equiv \frac{d^3\sigma(e^- + N_A \rightarrow J + X)}{dy dP_{J_T} d\tau_1}, \quad (2)$$

where the cross-section is differential in τ_1 and the transverse momentum (P_{J_T}) and rapidity (y) of the jet. This observable was explored in the region of phase space characterized by the restriction

$$\tau_1 \ll P_{J_T}, \quad (3)$$

which is effectively an inclusive veto on additional jets. A typical event corresponding to this region of phase space is schematically shown in Fig. 1. It corresponds to a

single narrow jet with only soft radiation of energy $E \sim \tau_1 \ll P_{J_T}$ allowed between the beam and jet directions. The physics of this region of phase space is dominated by collinear emissions along the beam and jet directions and soft emissions throughout the event. Large Sudakov logarithms appear of the form $\alpha_s^n \ln^m(P_{J_T}/\tau_1)$ for $m \leq 2n$ and correspond to the jet-veto logarithms. The Soft-Collinear effective theory (SCET) ^{19,20,21,22,23,24}, is the appropriate effective theory for this region of phase space and facilitates a resummation of the Sudakov logarithms within a factorization framework.

Such a factorization framework for the process in Eq.(2), in the region $\tau_1 \ll P_{J_T}$, was first derived in Ref. 18. Numerical results were presented for a proton target at the NLL level of accuracy. In Ref. 25, results were extended to include resummation at next-to-next-to-leading logarithmic (NNLL) level of accuracy, for a variety of nuclear targets. This was the first time that NNLL resummation was achieved for a DIS event shape. Subsequently, 1-jettiness for DIS was studied in Ref. 26 and they also independently presented results at NNLL level of accuracy for the proton target. They studied three different versions of 1-jettiness for DIS which they denoted as τ_a, τ_b , and τ_c . These different versions correspond to different choices for the reference vectors, used to define the 1-jettiness event shape, and have correspondingly different factorization structures as presented in Ref. 26. The event-shape τ_a is equivalent to τ_1 first studied in Refs. 18, 25, τ_b was shown to be equivalent to the thrust distribution studied in Ref. 1, and τ_c is a new definition of 1-jettiness that is naturally conducive for analysis in the target rest frame. Together with the works of Refs. 1, 2, 3, 4, 18, 25, 26, a large class of DIS event shapes have now been explored. These works can be viewed as complementary to each other, as they provide independent quantitative measures of the properties of the final-state QCD radiation in DIS processes.

2. Formalism

Here we focus on the work of Refs. 18, 25. The cross-section in Eq.(2) is computed in the center of mass frame (see Fig. 1) defined by the electron momentum and the *average* nucleon momentum in the nucleus. The momentum of the incoming electron (p_e) and the nucleus (P_A) can then be written as $p_e^\mu = (p_e^0, \vec{p}_e)$, $P_A^\mu = A(p_e^0, -\vec{p}_e)$ so that the electron and nucleus are treated as massless $p_e^2 = 0$. By setting $p_e^0 = |\vec{p}_e| = Q_e/2$, the center of mass energy is given by

$$s = (p_e + P_A)^2 = A Q_e^2. \quad (4)$$

The 1-jettiness event shape is defined as

$$\tau_1 = \sum_k \min \left\{ \frac{2q_A \cdot p_k}{Q_a}, \frac{2q_J \cdot p_k}{Q_J} \right\}, \quad (5)$$

where the sum is over all final state particles (except the lepton) with momenta denoted by p_k . The null vectors q_A and q_J denote reference vectors along the nuclear

beam and jet directions respectively. The parameters Q_a and Q_J are on the order of the hard scale P_{J_T} and different choices correspond to different definitions of τ_1 . The reference vectors q_A and q_J can be determined via a minimization²⁸ condition such that the optimal choice minimizes the value of τ_1 . In this procedure, the analysis can be performed without reference to any jet algorithm and is analogous to finding the thrust axis in the calculation of thrust distributions. One can also choose q_A to align with the beam axis and determine q_J via a standard jet algorithm. Note that in this case, the only information from the jet algorithm that is used in the calculation of τ_1 is the corresponding determination of the reference vector q_J . τ_1 has no explicit dependence on other jet algorithm parameters such as the jet radius R . This property of the event shape formalism allows for better analytic control over higher order perturbative corrections.

From Eq.(5), we see that energetic radiation at wide angles from the beam (q_A) and jet (q_J) directions make the largest contributions to τ_1 . Thus, by restricting to the region $\tau_1 \ll P_{J_T}$, energetic radiation ($E \sim P_{J_T}$) is only allowed along the beam and jet directions. This corresponds to the picture shown schematically in Fig.1, where the radiation at wide angles from the beam and jet directions is restricted to be soft ($E \sim \tau_1 \ll P_{J_T}$). Thus, in this region the dependence of any jet algorithm will be associated with how soft radiation at wide angles is grouped into the jet. This effect in determining the reference vector q_J is thus power suppressed in τ_1/P_{J_T} .

For our numerical analysis, we choose the reference vectors q_A and q_J as

$$q_A^\mu = x_A P_A^\mu, \quad q_J^\mu = P_J^\mu = (P_{J_T} \cosh y, \vec{P}_{J_T}, P_{J_T} \sinh y), \quad (6)$$

where x_A is the nucleus momentum fraction carried by the incoming parton that enters the hard interaction, and P_J is the total momentum of the final-state jet. Thus, the reference vector q_J is simply defined as the massless vector constructed from the differential quantities P_{J_T} and y in the cross-section in Eq.(2). For the parameters Q_a and Q_J we choose

$$Q_a = x_A A Q_e, \quad Q_J = 2P_{J_T} \cosh y. \quad (7)$$

The total jet momentum is defined as

$$P_J = \sum_k p_k \theta\left(\frac{2q_A \cdot p_k}{Q_a} - \frac{2q_J \cdot p_k}{Q_J}\right). \quad (8)$$

This definition is closely related to 1-jettiness. From Eq.(5), it is clear that each final state hadronic particle of momentum p_k is associated either with the beam (q_A) or jet (q_J) directions through minimization condition in Eq.(2). The total jet momentum is defined as the sum of the momenta of all particles associated with the q_J direction, as quantified by the step function in Eq.(8). In the region $\tau_1 \ll P_{J_T}$, the total jet momentum (and correspondingly q_J) obtained from a different jet algorithm, will differ by power corrections in τ_1/P_{J_T} associated with how wide-angle soft radiation is grouped into the jet.

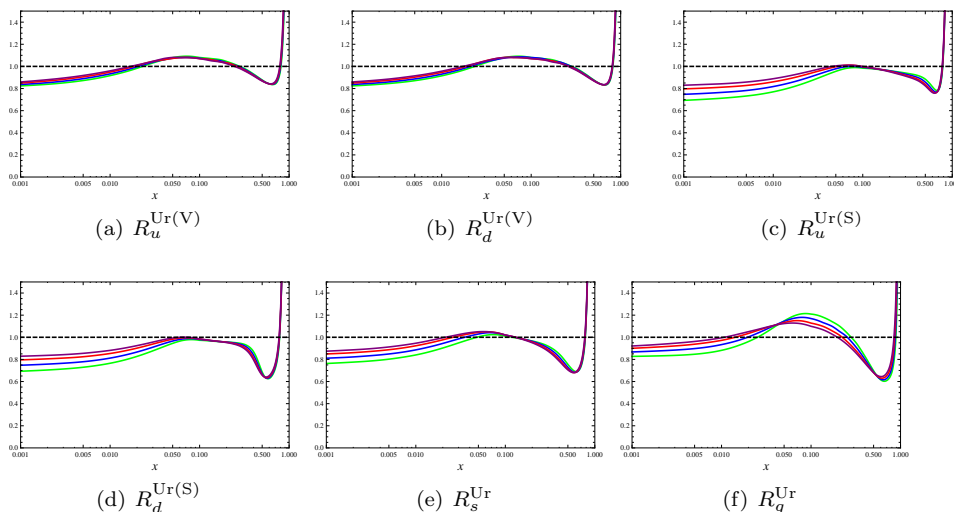


Fig. 2. Nuclear correction factors $R_i^{\text{Ur}}(x, \mu)$ for the NLO nuclear PDF for a Uranium target as defined in Eq.(13). The subscript i runs over the parton species $i = \{u, d, s, g\}$. For the u and d quarks, separate R -factors are given for the valence (V) and sea quarks (S). The different curves in each graph correspond to different values for the scale μ . By looking at the region of small Bjorken- x , the different curves from the bottom to the top correspond to $\mu = 3$ GeV (Green), $\mu = 5$ GeV (Blue), $\mu = 10$ GeV (Red), and $\mu = 20$ GeV (Purple). These plots were generated using publicly available code for the EPS09 PDF set.

The factorization formula^{18,25} for the observable in Eq.(2) has the schematic form

$$\frac{d^3\sigma}{dydP_{J_T}d\tau_1} \sim H \otimes B \otimes J \otimes S, \quad (9)$$

where H, B, J , and S (see Fig. 1) denote the hard, nuclear beam, jet, and soft functions respectively. The hard function is associated with the hard partonic interaction that produces the final-state jet. The beam function¹⁴ captures the physics of the initial state parton distributions and correlations in the nucleus, energetic ($E \sim P_{J_T}$) initial-state collinear radiation, and beam remnants. The jet function describes the dynamics of collinear radiation along the jet direction. Finally, the soft function describes the dynamics of soft ($E \sim \tau_1$) radiation throughout the event. All of these objects have well-defined field-theoretic definitions and can be found listed in Ref. 25. The beam function is sensitive to two disparate scales associated with the perturbative emissions of initial-state radiation and the non-perturbative physics of the initial state nucleus. The physics of these two scales can be separated¹⁴ through an operator product expansion (OPE) so that at leading twist, the beam function can be written as a convolution between a perturbatively calculable coefficient \mathcal{I}

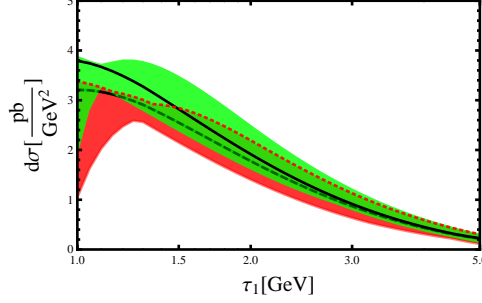


Fig. 3. τ_1 -distribution for a proton target with NLL' (lower red band) and NNLL (upper green band) resummation for $Q_e = 90$ GeV, $P_{J_T} = 20$ GeV and $y = 0$.

and the standard nuclear parton distribution function (PDF) (f_A)

$$B \sim \mathcal{I} \otimes f_A + \mathcal{O}\left[\frac{Q_s^2(A)}{\tau_1 P_{J_T}}\right]. \quad (10)$$

The coefficient \mathcal{I} describes the physics of the perturbative initial-state collinear emissions that knocks the initial parton off-shell by an amount $p^2 \sim \tau_1 P_{J_T}$. Power corrections in the OPE depend on the nuclear scale Q_s which depends on the nuclear species. The dependence of Q_s on the atomic weight of the nucleus is typically parameterized as

$$Q_s^2(A) \sim A^\alpha \Lambda_{QCD}^2, \quad (11)$$

where the parameter α depends on the details of the underlying nuclear physics. Thus, one can explore nuclear-dependent power corrections in the space of $\{A, P_{J_T}, \tau_1\}$, by looking for deviations from the predictions of the leading twist formula.

3. Numerical Results

The more detailed version of the schematic factorization formulae in Eqs.(9) and (10) is given by

$$\begin{aligned} d\sigma_A(\tau_1, P_{J_T}, y) &\equiv \frac{d^3\sigma}{dy dP_{J_T} d\tau_1} \Big|_{\text{EPS09}} = \sigma_0 \sum_{q,i} e_q^2 \int_{x_*}^1 \frac{dx}{x} \int ds_J \int dt_a \\ &\quad \times H(\xi^2, \mu; \mu_H) J^q(s_J, \mu; \mu_J) \mathcal{I}^{qi} \left(\frac{x_*}{x}, t_a, \mu; \mu_B \right) \\ &\quad \times \mathcal{S} \left(\tau_1 - \frac{t_a}{Q_a} - \frac{s_J}{Q_J}, \mu; \mu_S \right) f_{i/A}^{\text{EPS09}}(x, \mu_B), \end{aligned} \quad (12)$$

where we have used the EPS09²⁹ nuclear PDF set for generating numerical results. This is the master formula used for generating all numerical results at leading

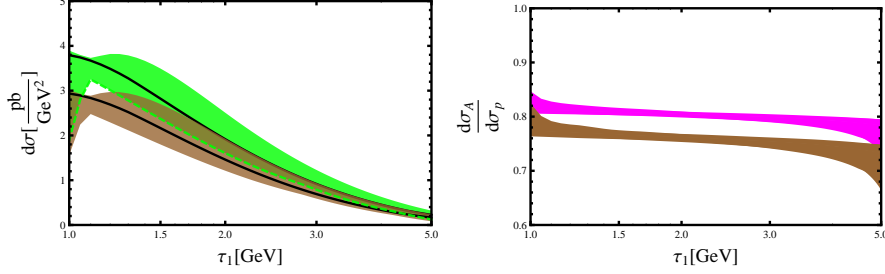


Fig. 4. Left Panel: τ_1 -distributions with NNLL resummation for the proton (upper green band) and Uranium (lower brown band) targets at $Q_e = 90$ GeV, $P_{J_T} = 20$ GeV, and $\tau_1 = 1.5$ GeV. Right Panel: Ratio of Uranium to proton (lower brown band) and Carbon to proton (upper magenta band) τ_1 -distributions at the same kinematics.

twist with NNLL resummation. For more details about this formula we refer the reader to the original paper in Ref. 25. Note that all of the nuclear dependence in the factorization formula is contained entirely in the nuclear PDFs $f_{i/A}$. All other objects are independent of the nuclear target giving rise to universality among processes with different nuclear targets. The nuclear PDFs are parameterized as

$$\begin{aligned}
 f_{u/A}^{EPS09}(x, \mu) &= \frac{Z}{A} R_u^A(x, \mu) f_{u/p}(x, \mu) + \frac{A-Z}{A} R_d^A(x, \mu) f_{d/p}(x, \mu), \\
 f_{d/A}^{EPS09}(x, \mu) &= \frac{Z}{A} R_i^A(x, \mu) f_{d/p}(x, \mu) + \frac{A-Z}{A} R_u^A(x, \mu) f_{u/p}(x, \mu), \\
 f_{s,c,b/A}^{EPS09}(x, \mu) &= R_{s,c,b}^A(x, \mu) f_{s,c,b/p}(x, \mu), \\
 f_{g/A}^{EPS09}(x, \mu) &= R_g^A(x, \mu) f_{g/p}(x, \mu),
 \end{aligned} \tag{13}$$

where Z denotes the atomic number of the nucleus, the $f_{i/p}$ denote the standard proton PDFs, and the R_i^A denote nuclear correction factors. Isospin symmetry has been used to write neutron PDFs in terms of proton PDFs. The nuclear correction factors parameterize well-known nuclear effects. Shadowing effects suppress the nuclear PDFs at small- x . On the other hand, anti-shadowing gives rise to an enhancement of the nuclear PDFs in the region $x \sim 0.1$. The EMC effect suppresses the parton density for moderate values $x > 0.2$ and the Fermi motion of nucleons causes an enhancement for large values of x . These effects are illustrated in Fig. 2 where nuclear correction factors for various parton densities are shown for the Uranium nucleus. As seen in Eq.(12), the nuclear PDFs are integrated over the range $[x_*, 1]$ where

$$x_* = \frac{e^y P_{J_T}}{Q_e - e^{-y} P_{J_T}}. \tag{14}$$

Thus, by exploring the kinematic space spanned by $\{Q_e, P_{J_T}, y\}$, one can gain sensitivity to different regions of Bjorken- x and probe the various nuclear effects.

In Fig. 3, we show the τ_1 distribution for a proton target at $Q_e = 90$ GeV, $P_{J_T} = 20$ GeV, and $y = 0$. We show numerical results for NLL+NLO, denoted as NLL'

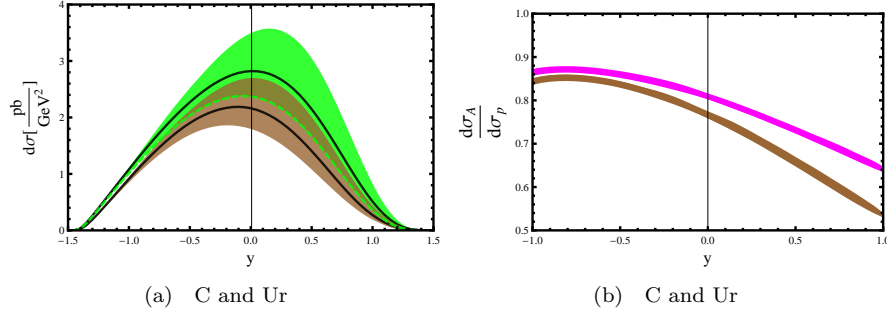


Fig. 5. Left Panel: Rapidity (y) distributions with NNLL resummation for the proton (upper green band) and Uranium (lower brown band) targets at $Q_e = 90$ GeV, $P_{J_T} = 20$ GeV, and $\tau_1 = 1.5$ GeV. Right Panel: Ratio of Uranium to proton (lower brown band) and Carbon to proton (upper magenta band) rapidity distributions at the same kinematics.

(lower red band), and NNLL resummation (upper green band). The resummation of the Sudakov logs of τ_1/P_{J_T} tames the singular behavior of the fixed order cross-section as one makes the jet-veto more and more restrictive by going to the region of small τ_1 . The width of the bands estimate the perturbative uncertainty from higher order effects and are obtained by standard scale variation procedures. For $\tau_1 \sim \Lambda_{QCD}$, the universal soft function becomes non-perturbative must be modeled. For more details and numerical results for the region $\tau_1 \sim \Lambda_{QCD}$, we refer the reader to Ref. 25.

In the left panel of Fig. 4 we show the τ_1 distribution with NNLL resummation for the proton (upper green band) and Uranium (lower brown band). In the right panel we show the ratio of distributions. The lower brown band shows the ratio of the Uranium to proton τ_1 distribution. We also show the ratio of Carbon to proton distribution as the upper purple band. Note that there is a dramatic reduction in the scale variation uncertainties in the ratio of τ_1 distribution between different nuclear targets. These ratios also deviate from unity well outside the theoretical uncertainty bands showing that these distributions are effective probes of nuclear effects.

In the left panel of Fig. 5 we show the rapidity distributions with NNLL resummation for the proton (upper green band) and Uranium (lower brown band) targets at the fixed values of $\tau_1 = 1.5$ GeV, $Q_e = 90$ GeV, and $P_{J_T} = 20$ GeV. In the right panel we show the ratio of the Uranium to proton rapidity distributions (lower brown band). We also show the ratio of the Carbon to proton distributions. Once again, there is a dramatic reduction in the scale variation uncertainty in the ratio of distributions. In addition the ratio of rapidity distributions of different nuclear targets has an interesting shape corresponding to the fact that different values of rapidity probe different regions of Bjorken- x in the nuclear PDFs, as seen from Eq.(14).

We refer the reader to Ref. 25 for more detailed discussions and many more

numerical results that include a large variety of nuclear targets, distributions in the other kinematic variables P_{JT} and Q_e , and distributions in the non-perturbative soft region $\tau_1 \sim \Lambda_{QCD}$.

Acknowledgements

This work was supported in part by the U.S. Department of Energy under contract numbers DE-AC02-05CH11231 (ZK), DE-AC02-98CH10886 (JQ), DE-AC02-06CH11357 (XL) and the grants DE-FG02-95ER40896 (XL) and DE-FG02-08ER4153 (XL), and the U.S. National Science Foundation under grant NSF-PHY-0705682 (SM).

References

1. V. Antonelli, M. Dasgupta and G. P. Salam, JHEP **0002**, 001 (2000).
2. M. Dasgupta and G. P. Salam, Phys. Lett. B **512**, 323 (2001)
3. M. Dasgupta and G. P. Salam, Eur. Phys. J. C **24**, 213 (2002)
4. M. Dasgupta and G. P. Salam, JHEP **0203**, 017 (2002)
5. S. Catani and M. H. Seymour, Nucl. Phys. B **485**, 291 (1997) [Erratum-ibid. B **510**, 503 (1998)]
6. D. Graudenz, hep-ph/9710244.
7. C. Adloff *et al.* [H1 Collaboration], Phys. Lett. B **406**, 256 (1997).
8. A. Aktas *et al.* [H1 Collaboration], Eur. Phys. J. C **46**, 343 (2006).
9. C. Adloff *et al.* [H1 Collaboration], Eur. Phys. J. C **14**, 255 (2000) [Erratum-ibid. C **18**, 417 (2000)]
10. J. Breitweg *et al.* [ZEUS Collaboration], Phys. Lett. B **421**, 368 (1998).
11. S. Chekanov *et al.* [ZEUS Collaboration], Eur. Phys. J. C **27**, 531 (2003)
12. S. Chekanov *et al.* [ZEUS Collaboration], Nucl. Phys. B **767**, 1 (2007)
13. I. W. Stewart, F. J. Tackmann and W. J. Waalewijn, Phys. Rev. Lett. **105**, 092002 (2010).
14. I. W. Stewart, F. J. Tackmann, and W. J. Waalewijn, Phys.Rev. **D81**, 094035 (2010).
15. I. W. Stewart, F. J. Tackmann, and W. J. Waalewijn, Phys.Rev.Lett. **106**, 032001 (2011).
16. X. Liu, S. Mantry and F. Petriello, Phys. Rev. D **86**, 074004 (2012).
17. T. T. Jouttenus, I. W. Stewart, F. J. Tackmann and W. J. Waalewijn, arXiv:1302.0846 [hep-ph].
18. Z. -B. Kang, S. Mantry and J. -W. Qiu, Phys. Rev. D **86**, 114011 (2012)
19. C. W. Bauer, S. Fleming, and M. E. Luke, Phys.Rev. **D63**, 014006 (2000), hep-ph/0005275.
20. C. W. Bauer, S. Fleming, D. Pirjol, and I. W. Stewart, Phys.Rev. **D63**, 114020 (2001), hep-ph/0011336.
21. C. W. Bauer and I. W. Stewart, Phys.Lett. **B516**, 134 (2001), hep-ph/0107001.
22. C. W. Bauer, D. Pirjol, and I. W. Stewart, Phys.Rev. **D65**, 054022 (2002), hep-ph/0109045.
23. C. W. Bauer, S. Fleming, D. Pirjol, I. Z. Rothstein, and I. W. Stewart, Phys.Rev. **D66**, 014017 (2002), hep-ph/0202088.
24. M. Beneke, A. Chapovsky, M. Diehl, and T. Feldmann, Nucl.Phys. **B643**, 431 (2002), hep-ph/0206152.
25. Z. -B. Kang, X. Liu, S. Mantry and J. -W. Qiu, arXiv:1303.3063 [hep-ph].

26. D. Kang, C. Lee and I. W. Stewart, arXiv:1303.6952 [hep-ph].
27. T. T. Jouttenus, I. W. Stewart, F. J. Tackmann, and W. J. Waalewijn, Phys.Rev. **D83**, 114030 (2011), 1102.4344.
28. J. Thaler and K. Van Tilburg, JHEP **1202**, 093 (2012), 1108.2701.
29. K. Eskola, H. Paukkunen, and C. Salgado, JHEP **0904**, 065 (2009), 0902.4154.